RSC Advances

PAPER

View Article Online
View Journal | View Issue

Cite this: *RSC Adv.*, 2023, **13**, 16285

Effects of organoclay on colorless and transparent polyimide nanocomposites: thermomechanical properties, morphology, and optical transparency

Yeji Na,[a] Lee Ku Kwac,[ab] Hong Gun Kim,[ab] Yong Lak Joo [c] and Jin-Hae Chang *[b]

Received 19th March 2023
Accepted 16th May 2023

DOI: 10.1039/d3ra01809a

rsc.li/rsc-advances

Although aromatic polyimide (PI) exhibits excellent mechanical performance and thermal stability, its dark color limits applicability in optical displays. Therefore, it is desirable to manufacture colorless, transparent PI (CPI) nanocomposite films that retain excellent physical properties. In this study, a solution intercalation method was used to disperse organoclay (Cloisite 25A; CS25A) in poly(amic acid), which was prepared using 4,4′-oxydiphthalic dianhydride and 3,4′-oxydianiline as monomers. This dispersion was then subjected to thermal imidization to synthesize CPI hybrid films. The influence of the CS25A content (0–1.00 wt%) on the thermomechanical properties, optical transmittance, and morphology of the prepared films was investigated. The hybrid film with a CS25A content of 0.50 wt% exhibited the best thermomechanical properties. However, upon further increasing the organoclay content to 1.00 wt%, the physical properties deteriorated. At 0.50 wt% CS25A, some agglomeration occurred but most of the clay was well dispersed as nano-sized particles, as revealed by transmission electron microscopy. In contrast, when the CS25A content exceeded a critical content, most of the clay was agglomerated and the physical properties were reduced. All the obtained CPI hybrid films were colorless and transparent, regardless of the organoclay content.

1. Introduction

Aromatic polyimide (PI) is an important super-engineered polymer with excellent mechanical properties and thermal stability at high temperatures. Consequently, aromatic PI has been widely used in electronic materials and in the aerospace and military fields.[1–5] However, owing to the charge-transfer complex (CT-complex) effect resulting from intermolecular or intramolecular interactions between polymer chains, aromatic PI is inherently dark brown in color. In particular, when the PI main chain has a rigid-rod-type linear aromatic structure, which facilitates CT-complex formation, the color of PI becomes darker. For this reason, the utility of conventional PI in optical display applications is very limited, despite its advantageous properties.

To overcome this issue, several methods have been developed to fabricate colorless and transparent PI (CPI):[6,7] (1) incorporating monomers with a bent structure into the main chain to reduce the linearity of the structure, (2) introducing substituents onto the main chain to prevent molecular stacking, and (3) introducing strong electron-withdrawing groups such as fluorine or sulfone groups. In general, CPI films with a low cut-off wavelength (λ_0) can be synthesized by using monomers that inhibit CT-complex formation or reduce intermolecular interactions.[8–10] Therefore, the method of synthesizing the CPI film mainly depends on the design of a new monomer capable of imide reaction and various reaction conditions.[11,12]

Glass is commonly used in electronic materials, including various types of display devices. Until recently, transparent and flexible indium tin oxide (ITO) glass has been widely applied in display substrates and microelectronics. However, the use of ITO glass as a general-purpose electronic material is complicated by the scarcity and high cost of indium.[7,13,14] In addition, glass is heavy, brittle, and sensitive to sudden temperature changes, making it difficult to process electronic devices at high temperatures. In particular, the glass substrate for the cover cannot be applied to foldable displays because they are fragile and breakable due to continuous shape changes during use.

Although CPI is difficult to mass-produce due to its complex synthesis method and low yield, CPIs can replace glass in electronic materials for displays because of their high optical transparency, and excellent thermomechanical properties. Advantageously, CPIs can also be used to produce inexpensive polymer films with various properties by designing suitable monomer structures.[12,14] Consequently, recent studies have focused on the application of CPIs in solar cell panels, transparent electrodes, and electronic device displays such as light-

[a]*Graduate School of Carbon Convergence Engineering, Jeonju University, Jeonju 55069, Korea*
[b]*Institute of Carbon Technology, Jeonju University, Jeonju 55069, Korea. E-mail: jhchang@jj.ac.kr*
[c]*Robert Fredrick Smith School of Chemical and Biomolecular Engineering, Cornell University, Ithaca, NY 14853, USA*

emitting diode (LED) display, electroluminescent displays (ELDs), and plasma display.[2,5,15] Therefore, CPIs are not only excellent polymer materials that can replace glass but also have utility in future electronic materials such as wearable electronic devices.[16–18]

Nanometer-sized organic–inorganic hybrids typically have better thermal and mechanical properties than conventional composites because interfacial adhesion is maximized. In particular, compared with common micro-scale polymer composites, polymer/clay hybrids have superior physical properties, even if only a small amount of clay is added. In addition, in polymer/clay hybrids, the properties are greatly affected by the dispersion and exfoliation degree of clay.[19,20] Clay montmorillonite (MMT) has a layered structure with a large surface area of 700–800 $m^2\ g^{-1}$. Each layer is 1 nm thick and has a wide plate shape with an aspect ratio (length/width) of approximately 218.[21,22] However, pristine MMT is hydrophilic and has poor dispersibility in or compatibility with lipophilic polymers. Therefore, to increase bonding strength, it is necessary to replace MMT with an appropriate organic agent. When organically modified clay (organoclay) is dispersed in a polymer matrix and used as a nanofiller, the thermodynamic properties, gas barrier performance, and chemical resistance are greatly improved owing to attractive forces between the organoclay and polymer. The characteristics of organoclay allow such hybrids to be applied not only to sensors, electrodes, and nonlinear optical materials but also to printed circuit boards (PCBs) that require high gas barrier properties and high thermal stability, flat plate or flexible display films that require high optical transparency, and electronic products that require high strength and mechanical properties.[22–24]

In this study, *meta*-substituted 4,4′-oxydiphthalic dianhydride (ODPA) and 3,4′-oxydianiline (ODA) monomers were used to design a CPI structure with a bent main chain containing freely rotating ether functional groups to prevent CT-complex formation and increase optical transparency. Poly(amic acid) (PAA) was synthesized using ODPA and ODA under low-temperature conditions, and then CPI hybrid films were prepared *via* a solution intercalation method by dispersing an organoclay in PAA followed by heat treatment at various temperatures and times. Cloisite 25A (CS25A) was used as the organoclay, and the content of dispersed CS25A was varied from 0 to 1.00 wt%. To determine the application potential of these CPI hybrid films, the thermomechanical characteristics, optical transparency, and morphology were evaluated according to the degree of organoclay dispersion in the CPI matrix.

2. Experimental

2.1. Materials

The ODPA and ODA monomers used for CPI synthesis were purchased from TCI (Tokyo, Japan). The solvent *N*,*N*′-dimethylacetamide (DMAc) was purchased from Junsei (Tokyo, Japan), and then molecular sieves (4 Å) were added to completely remove moisture. Organoclay CS25A was purchased from Southern Clay (Gonzales, USA).

2.2. Syntheses of PAA and CPI hybrid films

PAA was synthesized from ODPA and ODA in DMAc under low-temperature conditions, as follows: ODPA (17.28 g, 5.57×10^{-2} mol) and DMAc (100 mL) were placed in a three-necked flask, and this mixture was reacted at 0 °C for 0.5 h under N_2 gas. A mixture of DMAc (100 mL) and ODA (11.15 g, 5.57×10^{-2} mol) was added to the ODPA solution. The combined solutions were vigorously stirred at 0 °C for 1 h and then reacted at 25 °C for 14 h.

The CPI hybrid synthesis method was identical for each organoclay content. Therefore, the method for manufacturing a CPI hybrid film containing 0.50 wt% of CS25A is described as a representative example. First, 0.15 g of CS25A, 30 g of PAA solution, and excess DMAc (100 mL) were placed in a beaker and dispersion was achieved by vigorous stirring at room temperature for 2 h. The solution was then poured onto a glass plate, stabilized at 50 °C for 2 h, and dried in a vacuum oven at 80 °C for 1 h. Heat treatment of the PAA hybrid at 100, 150, and 200 °C for 1 h each, at 250 °C for 2 h, and finally at 300 °C for 30 min gave a CPI hybrid film with a thickness of 81 μm. The synthetic route is briefly shown in Scheme 1, and the detailed thermal imidization conditions for preparing the CPI hybrid films are summarized in Table 1. The synthesis of CPI hybrid films with more than 1.00 wt% organoclay was also attempted. However, bubbles were generated during polymerization and the samples broke into several pieces. Thus, it is believed that excess organoclay prevents the formation of CPI hybrid films.

2.3. Characterization

To confirm the structure of CPI, functional groups were identified using Fourier transform-infrared (FT-IR) spectroscopy (PerkinElmer, L-300, London, UK) in the range of 4000–1000 cm^{-1}. The CPI structure was also verified using ^{13}C-nuclear magnetic resonance (NMR) spectroscopy (^{13}C-NMR).

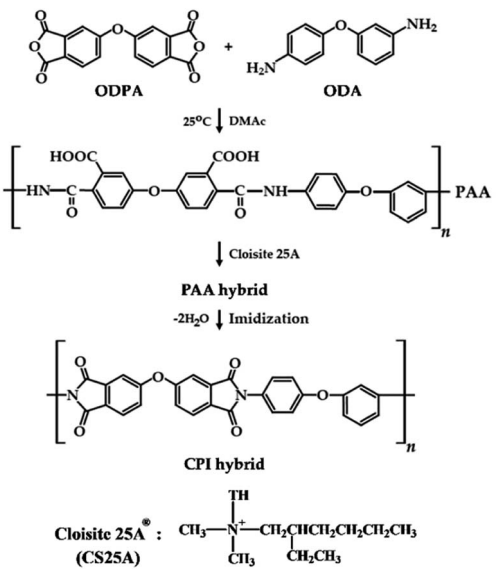

Scheme 1 Synthetic route for the preparation of CPI hybrid films.

Table 1 Heat treatment conditions for CPI hybrid films

Sample	Temp., °C/time, h/pressure, torr
PAA	0/1/760 → 25/14/760
PAA hybrid	25/2/760 → 50/2/760 → 80/1/1
CPI hybrid	100/1/760 → 150/1/760 → 200/1/760 → 250/2/760 → 300/0.5/760

Solid-state ^{13}C cross-polarized (CP)/magic angle spinning (MAS) NMR spectroscopy (Bruker 400 DSX, Berlin, Germany) was performed using a Larmor frequency of 100.61 MHz.

Wide-angle X-ray diffraction (XRD) was measured using a X-ray diffractometer (Rigaku, D/Max-IIIB, Tokyo, Japan) with Ni-filtered Cu-Kα radiation at a scan rate of 2° min^{-1} in the range $2\theta = 2$–12°. The dispersion morphology of the clay in the hybrid films was observed in detail using field emission scanning electron microscopy (FE-SEM; JEOL, JSM-6500F, Tokyo, Japan). For FE-SEM measurements, the CPI hybrid film was broken in liquid nitrogen and then sputter coated with gold using an SPI sputter coater to increase the conductivity of the broken surface. The morphology of the clay dispersed in the CPI matrix was also investigated using transmission electron microscopy (TEM; JEOL, JEM 2100, Tokyo, Japan) at an acceleration voltage of 120 kV. For TEM measurements, an epoxy resin sample was prepared by curing at 70 °C for 24 h and then cut into 90 nm thick specimens with a microtome under vacuum conditions. In order to observe the detailed shape of the clay, it was observed while changing from a low magnification to a high magnification by fixing the position of the object visible on the microscope.

Differential scanning calorimetry (DSC; F3200 Netzsch, Munchen, Germany) and thermogravimetric analysis (TGA; TA Q-500, New Castle, USA) were used simultaneously to measure the thermal properties of the CPI hybrid films. The temperature was changed at a rate of 20 °C min^{-1} in a N_2 atmosphere. Thermal mechanical analysis (TMA; Seiko, TMA/SS100, Tokyo, Japan) was used to measure the coefficient of thermal expansion (CTE). The temperature was increased at 5 °C min^{-1} with a load of 0.1 N, and the calculated values were obtained in the range of 100–250 °C by secondary heating.

The mechanical tensile properties were measured using a universal tensile machine (Shimadzu, JP/AG-50KNX, Tokyo, Japan) at a crosshead speed of 5 mm min^{-1}. After performing at least 10 measurements for each specimen, values outside the error range were excluded and the rest were averaged.

Light transmittance (λ_0 and 500 nm^{trans}) and yellow index (YI) were measured using a UV-vis spectrometer (Shimadzu, UV-3600, Tokyo, Japan) and a spectrophotometer (Konica Minolta, CM-3600d, Tokyo, Japan), respectively.

3. Results and discussion

3.1. FT-IR and ^{13}C-NMR analysis

The syntheses of PAA and CPI were confirmed using FT-IR spectro-scopy (Fig. 1). The C=O stretching peaks at 1730 and 1634 cm^{-1} are due to the acid and amide groups of PAA, respectively. For CPI, the C=O peaks are shifted to higher wavenumbers, appearing at approximately 1778 cm^{-1} (C=O, in phase) and 1698 cm^{-1} (C=O, out of phase). In addition, the formation of the imide functional groups was confirmed by the appearance of a characteristic peak corresponding to C–N–C stretching at 1360 cm^{-1}.[25]

The structure of CPI was further verified using solid-state ^{13}C-NMR CP/MAS spectroscopy at room temperature (Fig. 2). Peaks corresponding to carbon in the aromatic ring (*a–d* in the structural formula) were observed at 118.66, 125.79, 133.51, and 158.57 ppm. A peak corresponding to the imide carbon (*e* in the structural formula) was observed at 165.89 ppm.[26] The chemical shifts of all carbons were consistent with the expected chemical structure.

3.2. XRD analysis

XRD can be used to determine the distance between molecular chains depending on the degree of filler dispersion in the polymer matrix. Fig. 3 shows the XRD patterns of pure CS25A and the CPI hybrids with various CS25A contents in the range of $2\theta = 2$°–12°. CS25A exhibited a characteristic peak at $2\theta = 4.54$° ($d = 19.44$ Å). This peak was not observed for the CPI hybrid film with 0.25 wt% CS25A. However, at 0.50 wt% CS25A, a very weak peak was observed at $2\theta = 6.24$° ($d = 14.15$ Å), and the intensity of this peak increased as the CS25A content increased to 1.00 wt%. The gradually increase in the intensity of this peak with increasing organoclay content is likely due to the aggregation of clay particles to form an intercalated structure without complete exfoliation in the polymer matrix.[27] The *d* value of the hybrid films (14.15 Å) was small than that of pure organoclay (19.44 Å) because the interlayer spacing of the polymer chains between the clay layers was reduced during the imidization process.[24]

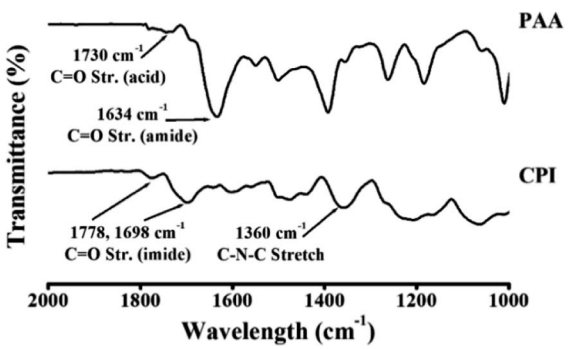

Fig. 1 FT-IR spectra of PAA and CPI.

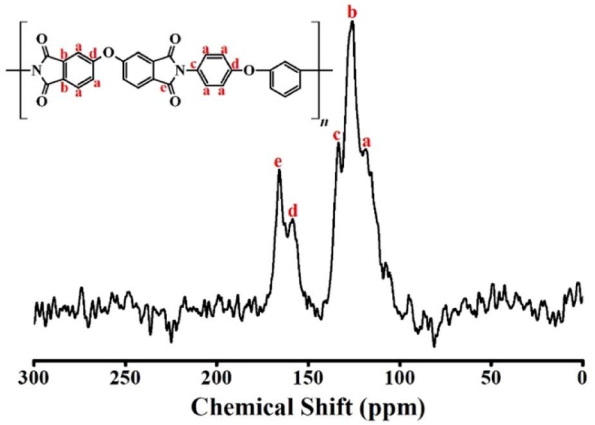

Fig. 2 ^{13}C-NMR spectrum of CPI.

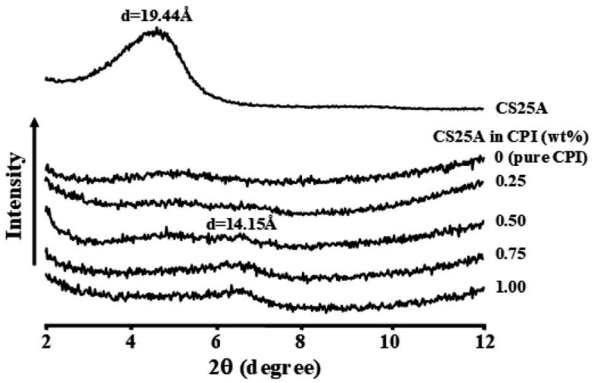

Fig. 3 XRD patterns of pure CS25A and CPI hybrids with various CS25A contents.

XRD provides a simple method for determining the distance between layers of clay dispersed in hybrid materials and has been widely used to evaluate clay agglomeration. However, for more accurate results, the detailed morphology of clay dispersed in a polymer matrix can be investigated using electron microscopy.[28,29]

3.3. Morphological analysis using electron microscopy

Electron microscopy observations can complement XRD results to reveal the detailed morphology of clay in hybrid films. FE-SEM was used to compare the fracture characteristics of pure CPI and the CPI hybrid films with various CS25A contents, whereas TEM was used to observe the specific shape and orientation of the dispersed clay particles.

As revealed by SEM imaging, no shape could be confirmed on the fracture surface of the pure CPI film without clay (Fig. 4(a)), but rough fracture surfaces were observed for the CPI hybrid films containing 0.25–1.00 wt% CS25A (Fig. 4(b)–(e)). The crown-shaped features on the rough fracture surfaces gradually decreased in size as the CS25A content increased to 1.00 wt%. This change occurs because the clay dispersed in the

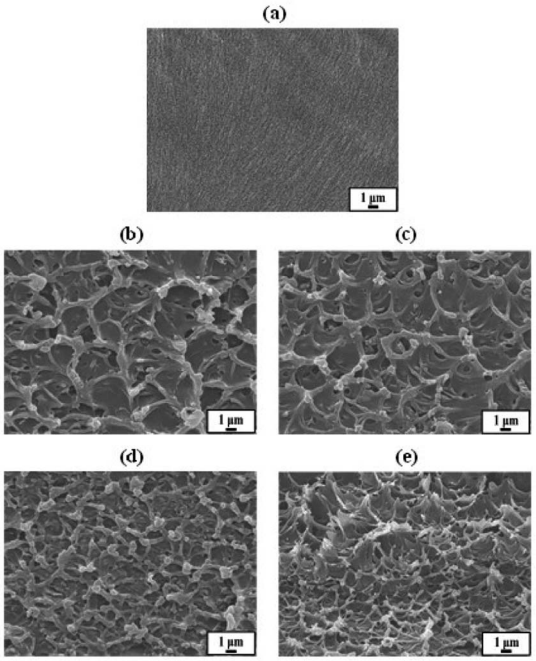

Fig. 4 SEM images of CPI hybrids containing (a) 0 (pure CPI), (b) 0.25, (c) 0.50, (d) 0.75, and (e) 1.00 wt% CS25A.

matrix acts as a nucleating agent and small crystalline domains are formed around the clay particles.[30]

Using TEM, it was possible to quantitatively explain the interlayer structure of the dispersed clay and the efficiency of its nanoscale dispersion within the CPI matrix. Fig. 5 and 6 show TEM images of the hybrids containing 0.50 and 1.00 wt% of CS25A, respectively. In each image, a black hair-like line is observed, which represents a 1 nm thick layer of clay, and the space between these lines represents the gap between the clay layers. In addition, the dispersed phase was observed in more detail by magnifying the region indicated by an arrow.

When the organoclay content in the hybrid film was 0.50 wt%, the clay was very well dispersed with an average thickness of less than 20 nm, as shown in Fig. 5. However, when the content of CS25A was increased to 1.00 wt%, the clay particles became more agglomerated, and nano-sized hybrids were formed in which the aggregated clay had an average thickness of less than 30 nm (Fig. 6). This result was consistent with the XRD results in Fig. 3. Excess clay above the critical

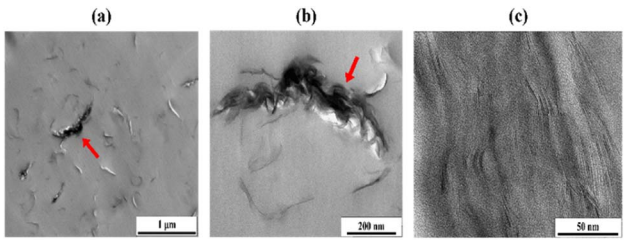

Fig. 5 TEM images of a CPI hybrid film containing 0.50 wt% CS25A with increasing magnification from (a) to (c).

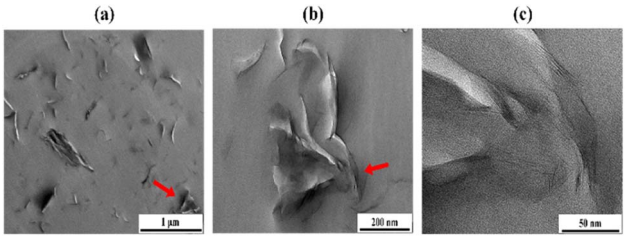

Fig. 6 TEM images of a CPI hybrid film containing 1.00 wt% CS25A with increasing magnification from (a) to (c).

content will have a detrimental effect on the thermomechanical properties and optical transparency of the hybrid film, as discussed below.

3.4. Thermal properties

The DSC results for the CPI hybrid films with various CS25A contents are summarized in Table 2, and the corresponding DSC thermograms showing the glass transition temperature (T_g) behavior are shown in Fig. 7. The T_g obtained in this study was determined by the on-set temperature of the secondary heated DSC curve. The T_g value of the pure CPI film was 279 °C. Upon adding organoclay, the T_g value initially increased and then decreased above a critical concentration. For example, when the CS25A content was 0.50 wt%, the T_g value increased to 289 °C. The increased T_g values of hybrids is due to two factors.[31,32] First, the small amount of clay layers dispersed in the CPI matrix affects the free volume. Second, the intercalation of polymer chains between the hard plate-like clay layers hinders movement, and T_g increases when the motion of chain segments is disturbed. However, when the content of CS25A was increased to 1.00 wt%, T_g decreased to 281 °C. Above the critical content, T_g decreased somewhat owing to the agglomeration of excess clay,[33,34] as demonstrated by the XRD and TEM results (see Fig. 3, 5, and 6).

The TGA thermograms of the CPI hybrid films with various organoclay contents are shown in Fig. 8. The behavior of the initial decomposition temperature (T_D^i) was similar to that of T_g. T_D^i increased from 471 to 496 °C when the CS25A content was increased from 0 to 0.50 wt% (Table 2). This increase occurred because the clay evenly dispersed in the CPI matrix effectively blocked the path of heat movement and suppressed the volatilization of the CPI component when a high

Table 2 Thermal properties of CPI hybrid films

CS25A in CPI (wt%)	T_g (°C)	$T_D^{i,a}$ (°C)	$wt_R^{800,b}$ (%)	CTE[c] (ppm/°C)
0 (pure CPI)	279	471	25	69
0.25	286	490	25	67
0.50	289	496	25	63
0.75	286	484	25	69
1.00	281	482	26	70

[a] At a 2% initial weight-loss temperature. [b] Weight percent of residue at 800 °C. [c] CTE obtained in the second heating cycle between 100 and 250 °C.

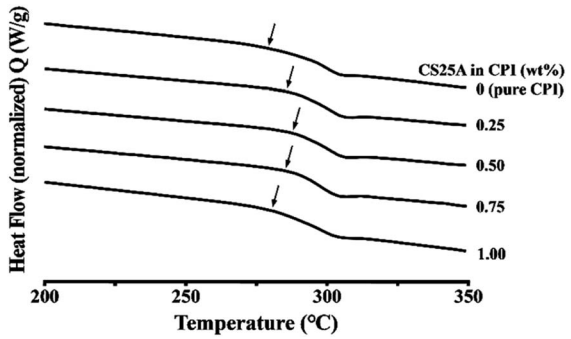

Fig. 7 DSC thermograms of CPI hybrids with various CS25A contents.

temperature was applied.[35–37] In contrast, when the organoclay content was increased to 1.00 wt%, T_D^i decreased to 482 °C. As higher organoclay contents, the thermal stability effect is somewhat inhibited because the excess clay is agglomerated and not evenly dispersed in the CPI matrix, as previously discussed. For the hybrids, the residual weight at 800 °C (wt_R^{800}) was constant (25–26%), regardless of the CS25A content. This is because the inorganic silicate remains after most of the organic components with low heat resistance in CS25A are decomposed at a high temperature of 800 °C.

When the hybrid is heated, the matrix PI chains relax in *a* direction perpendicular to the direction of propagation, but deformation of the filler clay is quite difficult. Consequently, the clay effectively blocks heat transfer, thus suppressing the thermal expansion of the PI matrix in the hybrid. To prepare a hybrid film with low thermal expansion, the filler must be effectively dispersed in the matrix polymer.[38–40] Table 2 summarizes the CTE values of the CPI hybrid films with various contents of organoclay after secondary heating in the temperature range of 100–250 °C, the corresponding TMA thermograms are shown in Fig. 9. The CTE values of the hybrid films decreased until a critical CS25A content was reached and then increased at higher CS25A contents. For example, the CTE value decreased from 69 to 63 ppm/°C upon increasing the CS25A content from 0 to 0.50 wt% but then increased to 69 ppm/°C at

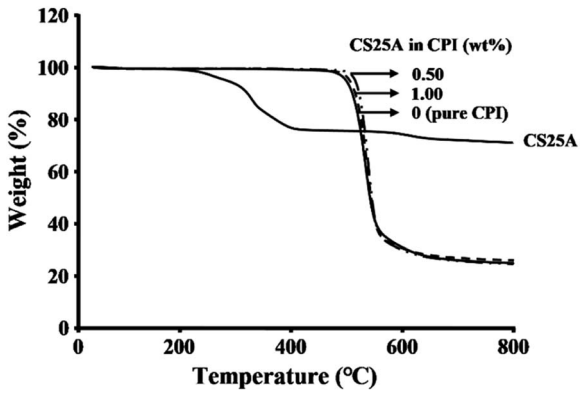

Fig. 8 TGA thermograms of pure CS25A and CPI hybrids with various CS25A contents.

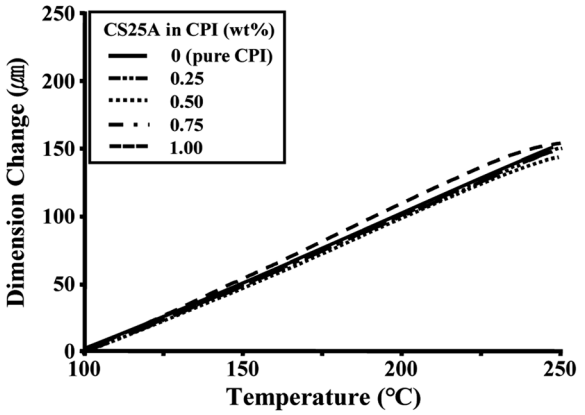

Fig. 9 TMA thermograms of CPI hybrids with various CS25A contents.

a CS25A content of 0.75 wt%. However, this value remained constant (70 ppm/°C) when the organoclay content was increased further to 1.00 wt%. The trends in the CTE values were consistent with the behavior of the T_g and $T_D{}^i$ values.

3.5. Mechanical properties

Fig. 10 shows the effect of the organoclay content on the mechanical properties of the CPI hybrid films, and Table 3 summarizes the mechanical properties of pure CPI and the CPI hybrid films with various organoclay contents. To increase the reliability of the results, all measurements were performed using hybrid films with similar thicknesses. The ultimate tensile strength of the pure CPI film was 93 MPa. With the dispersion of 0.50 wt% CS25A, the tensile strength increased by approximately 14% to 106 MPa, and the initial tensile modulus increased by approximately 30% from 2.09 to 2.69 GPa. In hybrids, the mechanical properties are critically affected by the dispersion and orientation of the fillers in the polymer matrix. This enhancement of the mechanical properties can be explained by the strength of the highly dispersed clay itself and the excellent orientation of the dispersed clay in the matrix.[41,42] However, when the CS25A content in the hybrid reached 1.00 wt%, both the tensile strength and initial modulus decreased (88 MPa and 2.27 GPa, respectively). This is because the agglomerates formed by excess clay above a critical content act like defects in the hybrid film,[43,44] as previously revealed by the XRD and TEM results. A constant elongation at break (EB) of 7–8% was observed for all the hybrid films, regardless of the organoclay content, owing to the reinforcing effect provided by the hard plate-like clay.

Table 3 Tensile properties of CPI hybrid films

CS25A in CPI (wt%)	Ult. str. (MPa)	Ini. mod. (GPa)	E.B.[a] (%)
0 (pure CPI)	93	2.09	8
0.25	99	2.45	7
0.50	106	2.69	8
0.75	102	2.47	8
1.00	88	2.27	7

[a] Elongation percent at break.

3.6. Optical transparency

The content of clay and the transmittance of light are closely related. That is, as the clay content of the matrix increases, the light transmittance of the composite material gradually decreases. This is because, as already explained, plate-shaped clay does not transmit light.[20]

The optical properties of the CPI hybrid films were evaluated using the values of λ_0 and the transmittance at 500 nm (500 nm^{trans}) in the visible region, which were determined using UV-vis spectroscopy, as well as the YI. The UV-vis spectra of the hybrid films are shown in Fig. 11, and the corresponding values are summarized in Table 4. To compare the optical properties under the same conditions, the thickness of each film was adjusted to 79–82 μm. The λ_0 value, which represents the initial transmission wavelength, was similar (315–316 nm) at each CS25A content (0–1.00 wt%). In addition, the 500 nm^{trans} values of all the CPI hybrid films were very high (96–98%), regardless of the CS25A content.

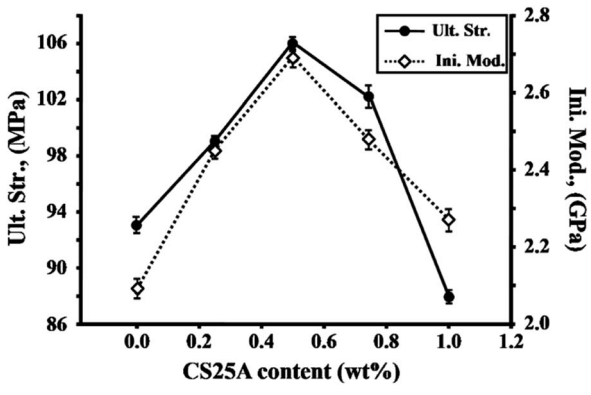

Fig. 10 Effect of CS25A content on the ultimate strength and initial modulus of CPI hybrid films.

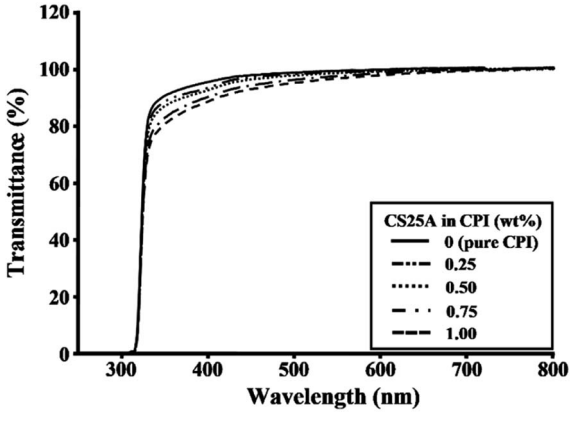

Fig. 11 UV-vis transmittance (%) of CPI hybrid films with various CS25A contents.

Table 4 Optical transparencies of CPI hybrid films

CS25A in CPI (wt%)	Thickness[a] (μm)	λ_0[b] (nm)	500 nm^{trans} (%)	YI[c]
0 (pure CPI)	80	315	98	1.2
0.25	82	316	97	1.1
0.50	81	316	97	1.1
0.75	79	316	96	1.5
1.00	81	316	96	1.5

[a] Film thickness. [b] Cut-off wavelength. [c] Yellow index.

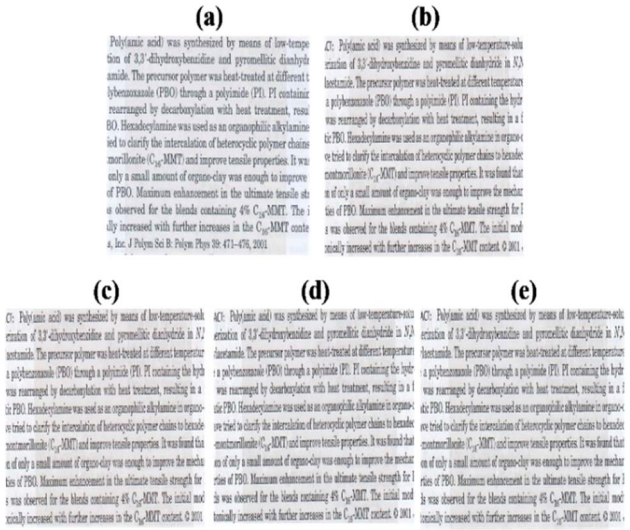

Fig. 12 Photographs of CPI hybrid films containing (a) 0 (pure CPI), (b) 0.25, (c) 0.50, (d) 0.75, and (e) 1.00 wt% CS25A.

Clay is a multi-layered mineral with one layer thickness of 1 nm, and when the concentration of clay increases and aggregates, it does not transmit light. However, when the clay is highly dispersed in the matrix and exfoliated to nanometer scale, the film exhibits colorless and transparent optical properties and at the same time exhibits a very low value of YI.[21,22] YI is calculated using the formula below (ASTM E313-96, DIN 6167):

$$YI = 100 \times (aX - bZ)/Y$$

where a and b are redness and yellowness, respectively. X, Y, and Z are tristimulus values.[45,46] The value of YI can be easily obtained using a spectrophotometer that automatically calculates the formula.

YI, which is a measure of the yellowness of a film, also revealed very good optical transparency regardless of the CS25A content (YI = 1.1–1.5), consistent with the 500 nm^{trans} results. The YI values obtained in this study are similar to that of poly(methyl methacrylate) (PMMA; YI = 1.2),[46] indicating that the CPI hybrid films are colorless and transparent, similar to glass. These results suggest that the clay has excellent dispersibility in the CPI matrix and is exfoliated to nano-sized particles, which do not interfere with light transmission, consistent with the TEM results (Fig. 5 and 6).

For the CPI film prepared in this study, the very low YI value indicates that CT-complex formation by π-electrons was prevented by introducing an *m*-substituted ether substituent that is bent and also capable of free rotation. To confirm the optical properties of the obtained films, photographs of the actual CPI hybrid films are shown in Fig. 12. As the hybrid films had similar YI values, regardless of the CS25A content, they were all colorless and transparent. Moreover, letters could be easily read through the prepared films.

4. Conclusions

In this study, CPI hybrid films were synthesized using a solution intercalation method, and the thermomechanical properties, morphology, and optical transparency of hybrid films with various CS25A contents were compared. All the hybrid films exhibited excellent optical transparency, and the optimal physical properties were observed at a CS25A content of 0.50 wt%.

The high interfacial adhesion between CPI and the nanofiller provided by uniform dispersion allows the fabrication of hybrid films with excellent physical properties that cannot be obtained using conventional processes. In addition, the nanoscale dispersion of a small amount of filler in CPI at a critical concentration provided a hybrid film with significantly improved physical properties. Owing to these enhanced properties, such hybrids have broad potential as film materials for electronic and optical applications.

Although traditional PI has been widely used in applications requiring high-performance films owing to its excellent thermomechanical properties, its dark color has limited applications in displays for electronic materials. As demonstrated in this study, this disadvantage can be overcome by synthesizing CPI using appropriately designed monomers, thus providing an advanced polymer material as a promising replacement for glass.

Author contributions

J.-H. Chang designed the project and wrote the manuscript. L. K. Kwac, H. G. Kim, and Y. L. Joo reviewed and data analyzed. Y. Na prepared the samples and participated in the data analysis. All authors have read and agreed to the published version of the manuscript.

Conflicts of interest

There are no conflicts to declare.

Acknowledgements

This research was supported by the Basic Science Research Program through the National Research Foundation of Korea (NRF) funded by the Ministry of Education (2016R1A6A1A03012069). This work also was supported by the National Research Foundation of Korea (NRF) grant funded the Korea government (MSIT) (2022R1A2C1009863).

References

1 Y. Guo, H. Qiu, K. Ruan, Y. Zhang and J. Gu, *Nano-Micro Lett.*, 2022, **14**, 1.
2 D.-J. Liaw, K.-L. Wang, Y.-C. Huang, K.-R. Lee, J.-Y. Lai and C.-S. Ha, *Prog. Polym. Sci.*, 2012, **37**, 907.
3 A. Shinji, M. Tohru and S. Shigekuni, *Polym. J.*, 1997, **29**, 69.
4 C. P. Feng, L. Bai, R.-Y. Bao, S.-W. Wang, Z. Liu, M.-B. Yang, J. Chen and W. Yang, *Compos. Commun.*, 2019, **12**, 80.
5 D. Lee, Y.-W. Lim, H.-G. Im, S. Jeong, S. Ji, Y. H. Kim, G.-M. Choi, J.-U. Park, J.-Y. Lee, J. Jin and B.-S. Bae, *ACS Appl. Mater. Interfaces*, 2017, **9**, 24161.
6 C.-J. Chen, H.-J. Yen, Y.-C. Hu and G.-S. Liou, *J. Mater. Chem. C*, 2013, **1**, 7623.
7 M.-C. Choi, Y. Kim and C.-S. Ha, *Prog. Polym. Sci.*, 2008, **33**, 581.
8 M. Nishihara, L. Christiani, A. Staykov and K. Sasaki, *J. Polym. Sci., Part B: Polym. Phys.*, 2014, **52**, 293.
9 M. Hasegawa, Y. Hoshino, N. Katsura and J. Ishii, *Polymer*, 2017, **111**, 91.
10 H.-J. Ni, J.-G. Liu, Z.-H. Wang and S.-Y. Yang, *J. Ind. Eng. Chem.*, 2015, **28**, 16.
11 H. Jeon, L. K. Kwak, H. G. Kim and J.-H. Chang, *Rev. Adv. Mater. Sci.*, 2022, **61**, 394.
12 J.-H. Chang, *Rev. Adv. Mater. Sci.*, 2020, **59**, 1.
13 J.-H. Kim, M.-C. Choi, H. Kim, Y. Kim, J.-H. Chang, M. Han, I. Kim and C.-S. Ha, *J. Nanosci. Nanotech.*, 2010, **10**, 388.
14 P. C. Wang and A. G. MacDiarmid, *Displays*, 2007, **28**, 101.
15 M. Kim, J. Park, S. Ji, S.-H. Shin, S.-Y. Kim, Y.-C. Kim, J.-Y. Kim and J.-U. Park, *Nanoscale*, 2016, **8**, 9504.
16 L. K. Kwac, H. G. Kim and J.-H. Chang, *ACS Omega*, 2021, **6**, 19006.
17 Y. Jung, S. Byun, S. Park and H. Lee, *ACS Appl. Mater. Interfaces*, 2014, **6**, 6054.
18 H. Xu, D. Luo, M. Li, M. Xu, J. Zou, H. Tao, L. Lan, L. Wang, J. Peng and Y. Cao, *J. Mater. Chem. C*, 2014, **2**, 1255.
19 J. X. Chan, J. F. Wong, M. Petrů, A. Hassan, U. Nirmal, N. Othman and R. A. Ilyas, *Polymers*, 2021, **13**, 2867.
20 J. W. Gilman, *Appl. Clay Sci.*, 1999, **15**, 31.
21 H. H. Murray, *Appl. Clay Sci.*, 1991, **5**, 379.
22 D. E. Abulyazied and A. Ene, *Polymers*, 2021, **13**, 4401.
23 K. Kwon and J.-H. Chang, *J. Compos. Mater.*, 2015, **49**, 3031.
24 H. I. Shin and J.-H. Chang, *Polymers*, 2020, **12**, 135.
25 D. L. Pavia, G. M. Lampman, G. S. Kriz and J. R. Vyvyan, *Introduction to Spectroscopy*, Cengage Learning, Boston, Massachusetts, USA, 2008, p. 14, ch. 2.
26 D. L. Pavia, G. M. Lampman, G. S. Kriz and J. R. Vyvyan, *Introduction to Spectroscopy*, Cengage Learning, Boston, Massachusetts, USA, 2008, p. 146, ch. 4.
27 K. Yano, A. Usuki, A. Okada, T. Kurauchi and O. Kamigaito, *J. Polym. Sci., Part A: Polym. Chem.*, 1993, **31**, 2493.
28 A. B. Morgan and J. W. Gilman, *J. Appl. Polym. Sci.*, 2002, **87**, 1329.
29 J. Ma, J. Xu, J.-H. Ren, Z.-Z. Yu and Y.-W. Mai, *Polymer*, 2003, **44**, 4619.
30 T. Oda, F. Kono and H. Saito, *Polym. Eng. Sci.*, 2012, **52**, 2228.
31 S. W. Kim and H. M. Choi, *High Perform. Polym.*, 2014, **27**, 694.
32 T. Agag and T. Takeichi, *Polymer*, 2000, **41**, 7083.
33 J.-H. Chang, B.-S. Seo and D.-H. Hwang, *Polymer*, 2002, **43**, 2969.
34 H. Xu, S.-W. Kuo, J.-S. Lee and F.-C. Chang, *Macromolecules*, 2002, **35**, 8788.
35 O. Becker, R. J. Varley and G. P. Simon, *Eur. Polym. J.*, 2004, **40**, 187.
36 J. Zhu, F. M. Uhl, A. B. Morgan and C. A. Wilkie, *Chem. Mater.*, 2001, **13**, 4649.
37 M. Y. Choi, S. J. Lee, A. R. Lim and J.-H. Chang, *Sci. Rep.*, 2022, **12**, 20892.
38 S. L.-C. Hsu, U. Wang, J.-S. King and J.-L. Jeng, *Polymer*, 2003, **44**, 5533.
39 F. Liu, Z. Liu, S. Gao, Q. You, L. Zou, J. Chen, J. Liu and X. Liu, *RSC Adv.*, 2018, **8**, 19034.
40 G. Qian, F. Dai, H. Chen, M. Wang, M. Hu, C. Chen and Y. Yu, *J. Polym. Sci.*, 2021, **59**, 510.
41 W. J. Bae, M. K. Kovalev, F. Kalinina, M. Kim and C. Cho, *Polymer*, 2016, **105**, 124.
42 T. Agag, T. Koga and T. Takeichi, *Polymer*, 2001, **42**, 3399.
43 S. Sequeira, D. V. Evtuguin and I. Portugal, *Polym. Compos.*, 2009, **30**, 1275.
44 M.-D. Damaceanu, C.-P. Constantin, A. Nicolescu, M. Bruma, N. Belomoina and R. S. Begunov, *Eur. Polym. J.*, 2014, **50**, 200.
45 C. H. Ju, J.-C. Kim and J.-H. Chang, *J. Appl. Polym. Sci.*, 2007, **106**, 4192.
46 C.-P. Yang and Y.-Y. Su, *Polymer*, 2005, **46**, 5778.